ACS APPLIED ENERGY MATERIALS

www.acsaem.org

Article

Thienothiophene and Triphenylbenzene Based Electroactive Conjugated Porous Polymer for Oxygen Reduction Reaction (ORR)

Recep Isci, Timuçin Balkan, Saeede Tafazoli, Berkay Sütay, Mehmet S. Eroglu, and Turan Ozturk*

Cite This: *ACS Appl. Energy Mater.* 2022, 5, 13284−13292

Read Online

ACCESS | Metrics & More | Article Recommendations | Supporting Information

ABSTRACT: Catalysts based on metal-free conjugated porous polymers (CPPs) are still rare for electrochemical oxygen reduction reactions (ORR). In this study, a conjugated porous polymer, **TT-TPB**, based on thieno[3,2-*b*]thiophene (TT) and triphenylbenzene (TPB), was synthesized applying palladium(0) catalyzed Suzuki coupling reaction and its ORR activity was investigated in alkaline condition. It demonstrated comparable electrocatalytic performance of ≈0.89−0.9 V E_{onset} vs RHE with the commercially available Pt/C. Density-functional theory (DFT) calculations revealed that **TT-TPB** featured efficient electrocatalytic active sites derived from volumetric, areal, and O_2 adsorbing calculations, which were in line with the experimental results. Moreover, semiconducting and surface properties of **TT-TPB** were investigated in detail using electrochemical and spectrophotometric techniques. This work shows the potential application of thienothiophene-based metal-free CPP in the electrochemical conversion process.

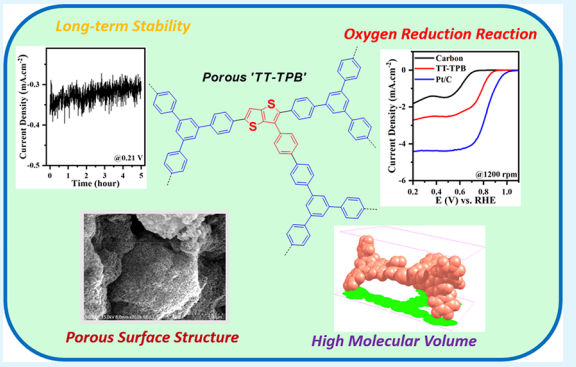

KEYWORDS: *thienothiophene, conjugated porous polymer (CPP), polymeric electrocatalyst, oxygen reduction reaction (ORR), metal-free electrocatalyst, catalyst kinetics*

INTRODUCTION

The growing energy crisis and consumption increase the interest in renewable and environmentally clean energy sources along with the conversion applications such as solar cells,[1−3] capacitors,[4,5] fuel cells,[6−9] and batteries.[10,11] Among these applications, fuel cells have important potential as an efficient energy source including oxygen reduction reaction (ORR) in a multielectron transfer process. However, ORR has highly sluggish kinetics leading to a reduced energy efficiency. To overcome this issue, highly active ORR electrocatalysts having high electroactive surface area are necessary for fabrication.[12−15] Although Pt-based materials are well-known catalysts for the ORR, they are not cost-effective for large-scale production since they suffer from serious anode crossover and limited stability.[16−18] Therefore, efforts have been mainly focused on the production of more stable and economically functional materials having catalytic activity with a larger surface area for ORR applications.[19−21]

Conjugated porous polymers (CPPs) have recently been categorized as a new class of electro/photoactive and heterogeneous catalysts, which can remove serious drawbacks of classic molecular catalysts, owing to their structural stability, low cost, nontoxicity, and easy designability.[22−25] Moreover, they offer many advantages such as permanent porous surface, flexible π-extended network, strong covalent links (e.g., aryl−aryl bond), adjustable band gap character, and photon absorption capability. Thus, CPPs with large pore surfaces and active edge sites have been considered one promising candidate for a high-performing ORR catalytic system.[23−27] In addition, they have been used in several electronic, optic, and catalytic applications to solve major challenges of sustainable energy and a clean environment.[28,29] Thienothiophenes are fused in two thiophene systems with four isomers, among which thieno[3,2-*b*]thiophene (TT) has the utmost importance as it has the best electron delocalization. It is electron-rich with two sulfur heteroatoms and flat and has remarkable optic/electronic and electrochemical oxidation/reduction properties.[30−44] Another important building block is 1,3,5-triphenylbenzene (TPB), which is a photochemically and thermally stable chromophore with a π-extended structure. As in TTs, TPB has a useful core for various electronic areas such as OLED, water splitting, triplet−triplet annihilation photon upconversion, and CO_2 photoreduction.[45−50] Since addition of sulfur has a positive impact in catalyzing the ORR,[51−54] combining a porous structure with a thiophene-based backbone may help to enhance the ORR activity.

Received: June 11, 2022
Accepted: October 18, 2022
Published: October 31, 2022

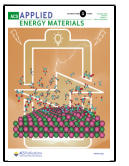

Scheme 1. Synthesis of Porous TT-TBP

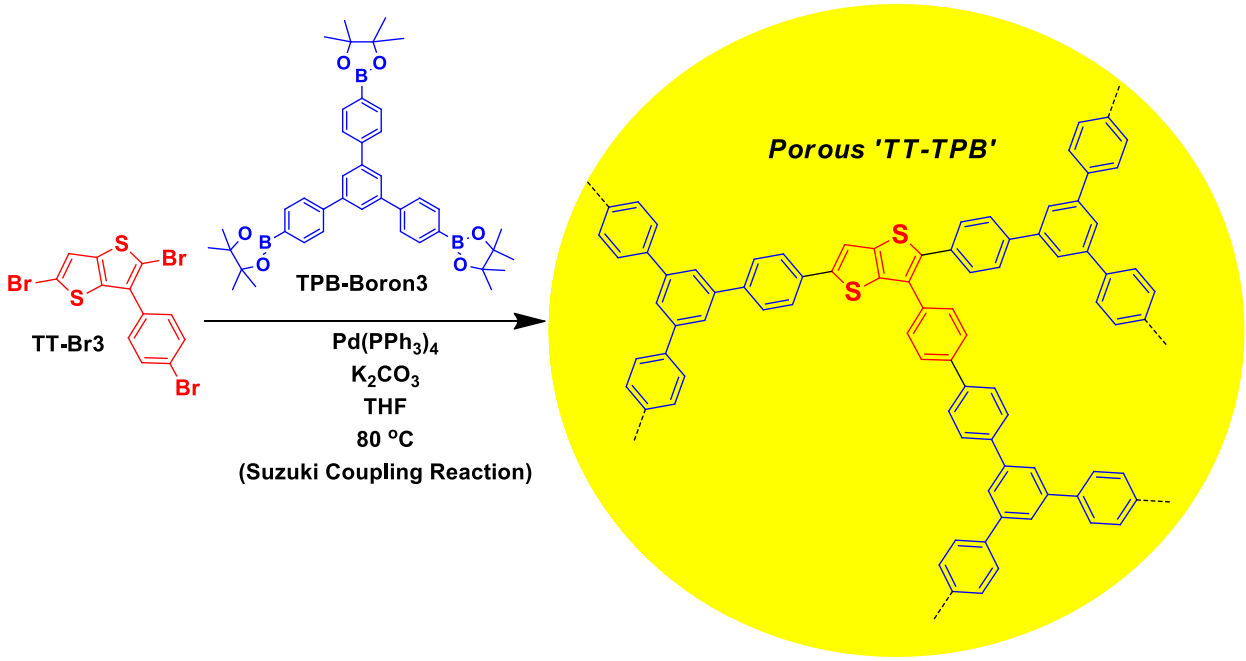

In this work, the design and synthesis of a novel porous conjugated polymer (**TT-TPB**) were described and characterized in detail. Moreover, the ORR performance of the material was investigated in alkaline conditions. Its electrocatalytic ORR activity was evaluated by using cyclic voltammetry (CV) and rotating disk electrode (RDE) methods. The surface morphology of **TT-TPB** was studied by scanning electron microscopy (SEM) to demonstrate its porous polymer morphology. This work shows the potential application of thieno[3,2-*b*]thiophene based metal-free CPP in the energy conversion process.

EXPERIMENTAL SECTION

Materials and Methods. All chemicals were used without further purification. Carbon black (Vulcan XC-72) and commercial Pt/C (20%) were supplied from Fuel Cell Store. Analytical grades of KOH, isopropyl alcohol, and Nafion solution (5 wt %) were supplied from Sigma-Aldrich. Electrochemical measurements were conducted in a three-electrode cell configuration. Ag/AgCl (4 M KCl, saturated) electrode as a reference electrode and Pt spiral wire as a counter electrode (CE) were applied. Also, a graphite (Gr) counter electrode was used to observe the contribution of Pt readsorbed nanoparticles of Pt CE (Figure S3). Since no significant changes were observed in CV and RDE measurements when graphite was used as the counter electrode, we continued with Pt CE. Regarding the working electrode, a catalyst-coated rotating carbon disk electrode (GC, 5 mm in diameter) was prepared as follows:

TT-TPB (5 mg/mL) and carbon black (5 mg/mL) were mixed with Nafion (40 μL) and Arabic gum (10 μL) in an isopropyl alcohol (480 μL)−water (480 μL) mixture. Arabic gum was used as a co-dispersant as it has a strong dispersion ability toward the conjugated systems.[55,56] To obtain a homogeneous dispersion, the mixture was kept in an ultrasonic bath and stirred. Finally, 10 μL of ink was dropped onto the GC and dried at room temperature. For comparison, the same recipe was applied for commercial Pt/C and pristine carbon black.

The ORR electrochemical activities were measured in KOH solution (0.1M) using a Pine Research WaveDriver 40 DC biopotentiostat/galvanostat with modulated speed rotator (MSR). The reference electrode was calibrated in H_2 purged H_2SO_4 (0.5 M) using Pt wire as a working electrode. All the measured potentials were converted to reversible hydrogen electrode using the equation below.

$$E_{(RHE)} = E_{Ag/AgCl} + 0.059\text{pH} + E^{o}_{Ag/AgCl}$$

The number of electrons involved in the ORR was calculated from the Koutecky−Levich (K-L) equation using the slope (B) of the graph between J^{-1} versus $\omega^{-1/2}$.

$$J^{-1} = J_L^{-1} + J_K^{-1} = (B\omega^{1/2})^{-1} + J_K^{-1} \quad (1)$$

$$B = 0.62nFC_0(D_0)^{2/3}\nu^{-1/6} \quad (2)$$

where J is the measured current density, J_K and J_L are the kinetic and diffusion-limiting current densities, ω is the angular velocity of the disk, n is the overall number of electrons transferred in oxygen reduction, F is the Faraday constant (F = 96485 C·mol^{-1}), C_0 is the bulk concentration of O_2, (C_0 = 1.2 × 10^{-6} mol·cm^{-1}), ν is the kinematic viscosity of the electrolyte (ν = 0.01 cm^2.s^{-1}), and D_0 is the diffusion coefficient of O_2 in 0.1 M KOH (1.9 × 10^{-5} cm^2·s^{-1}).[57]

Rotating ring disk electrode (RRDE) experiments were also performed at 1200 rpm with a scan rate of 10 mV·s^{-1} in 0.1 M O_2 saturated KOH to calculate electron transfer numbers. The related ring current was simultaneously measured using a Pt ring electrode, applying a constant potential of 1.1 V vs RHE. The electron transfer number and HO_2^-% were calculated using the equations below:[58]

$$n = 4\frac{I_D}{I_D + \frac{I_R}{N}} \quad (3)$$

$$HO_2^-\% = 200\frac{I_R/N}{I_D + I_R/N} \quad (4)$$

where I_D and I_R are the disk and ring currents, respectively, and N is the collection efficiency. The N value in our system was measured in 1 M KNO_3 with a 10 mM $K_3[Fe(CN)_6]$ electrolyte.

Mass corrected Tafel plots were calculated from the equation as follows:[59]

$$J_K = (J\cdot J_L)/(J_L - J)$$

The diffusion-limiting current densities (J_L) values were extracted from RDE voltammograms at 1200 rpm (at 0.2 V) and used directly in the formula.

https://doi.org/10.1021/acsaem.2c01830
ACS Appl. Energy Mater. 2022, 5, 13284−13292

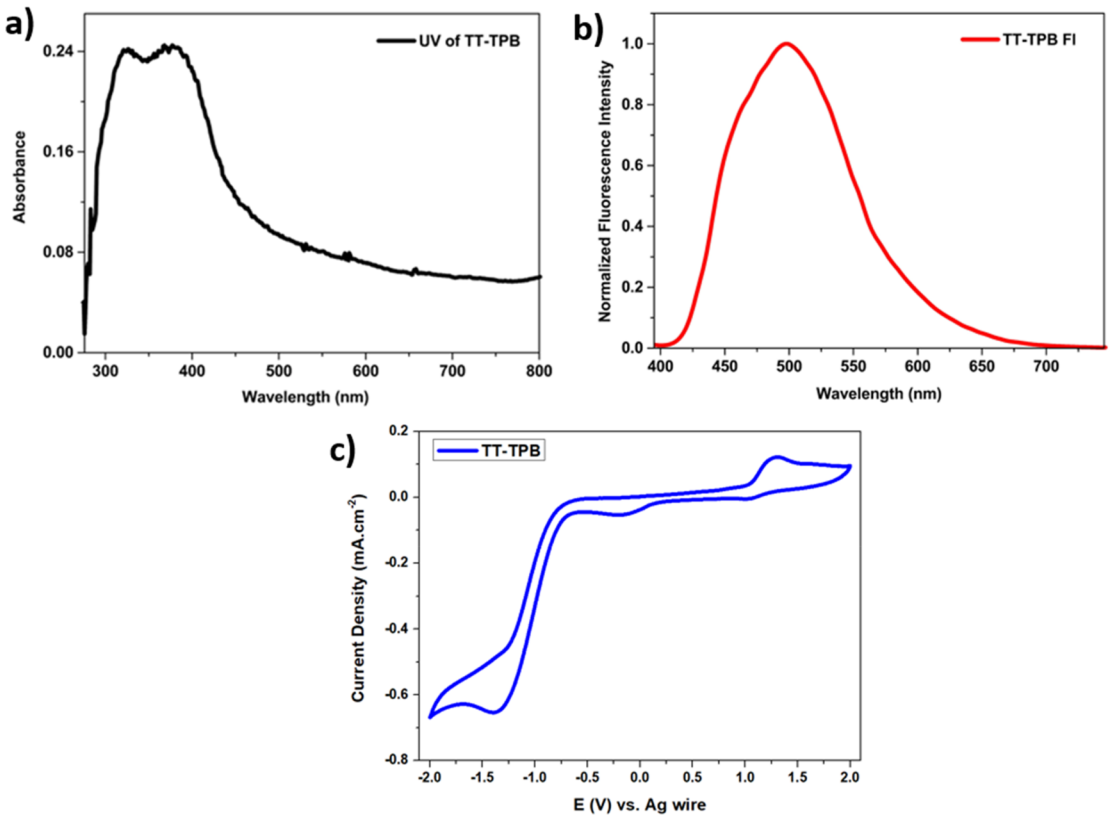

Figure 1. (a) Absorption, (b) emission spectra, and (c) cyclic voltammogram of **TT-TPB**.

Table 1. Optical and Electronic Data of TT-TPB

polymer	UV_{max}[a] (nm)	UV_{onset} (nm)	Fl_{max}[a] (nm)	Stokes shift (nm)	E_{optic}[b] (eV)	E_{ox} (V)	E_{red} (V)	E_{CV}[c] (eV)
TT-TPB	389	462	501	112	2.66	1.28	−1.35	2.63

[a]Absorption and emission maxima in THF. [b]E_{optic} from the onset of absorption spectra. [c]$E_{CV} = E_{ox} - E_{red}$.

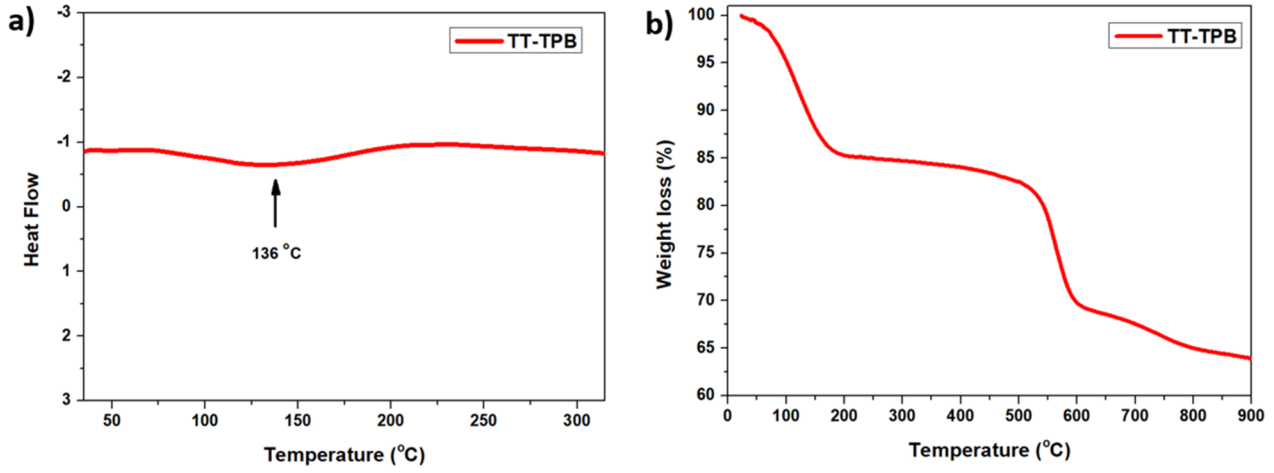

Figure 2. (a) DSC and (b) TGA thermograms of **TT-TPB**.

To determine the electrochemical band gap of **TT-TPB**, the cyclic voltammetric measurement was conducted in an acetonitrile/dichloromethane (4/1) mixture containing tetrabutylammonium hexafluorophosphate ($TBAPF_6$) (0.1 M) as a supporting electrolyte at a scan rate of 50 mV/s, using platinum (Pt) and silver (Ag) wires as working and reference electrodes, respectively. Cyclic voltammetry was examined on a Princeton Applied Research Versa STAT 3.

Scanning electron microscopy (SEM) images were recorded on a HITACHI SU 5000 VP-FEG-SEM&EDS, having Schottky gun at an acceleration voltage of 15 kV at different magnifications. Before the SEM operation, the sample was applied on a conductive double-sided adhesive carbon tape. Thermal gravimetric analysis (TGA) was performed on a PerkinElmer Diamond TA/TGA with a heating rate of 10 °C·min^{-1} under nitrogen flow. Differential scanning calorimetry (DSC) was conducted on a PerkinElmer Diamond DSC with a heating rate of 10 °C·min^{-1} under nitrogen flow, covering temperatures of 30−320 °C. BET equipment (NOVA 2200e BET) was used to measure the surface area of **TT-TPB**. Fourier-transform

https://doi.org/10.1021/acsaem.2c01830
ACS Appl. Energy Mater. 2022, 5, 13284−13292

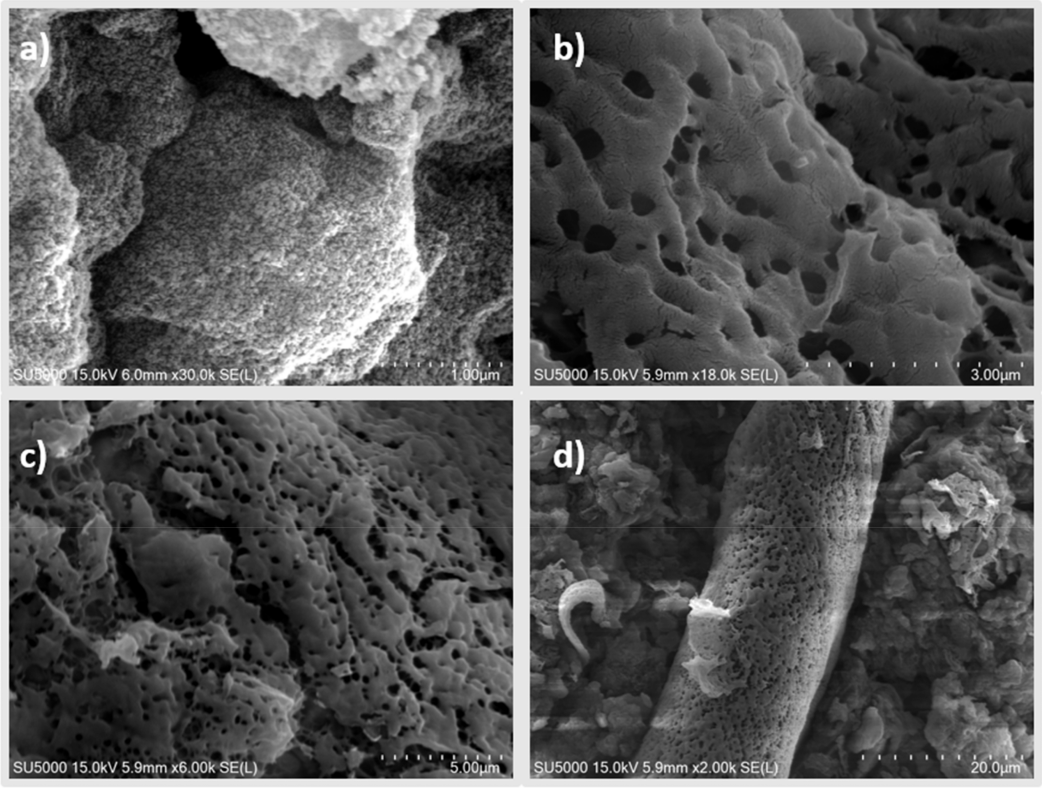

Figure 3. Scanning electron microscopy (SEM) images of **TT-TPB** at different magnifications (a–d).

infrared (FTIR) spectra were recorded on Perkin-Elmer Spectrum One spectrometer having an ATR accessory (ZnSe, Pike Miracle Accessory) and mercury cadmium telluride (MCT) detector.

Synthesis. **TT-Br3**[30] and **TPB-Boron3**[50] were synthesized following our previous and other literature reports.

Synthesis of TT-TPB. To a mixture of **TT-Br3** (0.3 g, 0.665 mmol) and **TPB-Boron3** (0.45 g, 0.665 mmol), dissolved in THF (25 mL) and degassed for 45 min with N_2, were added K_2CO_3 (2.5 mL, 2 M) and $Pd(PPh_3)_4$ (0.0065 mmol). The reaction was left stirring for 2 days at 90 °C, after which the precipitate was filtered and washed with various solvents (water, THF, methanol). Following a Soxhlet extraction in MeOH and THF (1 day each), it was dried under vacuum at 90 °C overnight to obtain the title compound as a brown powder in 85% yield. Porosity and apparent BET (Brunauer–Emmett–Teller) surface area of **TT-TPB** were evaluated by nitrogen isothermal adsorption/desorption measurements (Supporting Information, Figure S1, Table S1). On the basis of the N_2 adsorption isotherm at 77 K, the BET specific surface area of **TT-TPB** was calculated to be 69.91 m^2/g, indicating that **TT-TPB** has a typical microporous polymer nature (Scheme 1). FTIR (ATR, diamond) spectrum of **TT-TPB** displayed bands at 2367, 1592, 1509, 1183, 817, and 498 cm^{-1} (Figure S2).

RESULTS AND DISCUSSION

Photophysical properties (UV–vis and fluorescence) of **TT-TPB** were investigated in THF dispersed solution (Figure 1a,b, Table 1) since the **TT-TPB** is not soluble in THF as expected. While the maximum $\pi-\pi^*$ absorption wavelength (λ_{max}) of **TT-TPB** was 389 nm, its maximum emission wavelength appeared at 501 nm (ex. at λ_{max}), producing a mega Stokes shift of 112 nm, which could be due to a fast relaxation from the excited state to the ground state as a result of intramolecular energy-transfer between the conjugated groups. The optical band gap (E_{optic}) of **TT-TPB** was calculated as 2.66 eV from the onset wavelength of the absorption spectra.

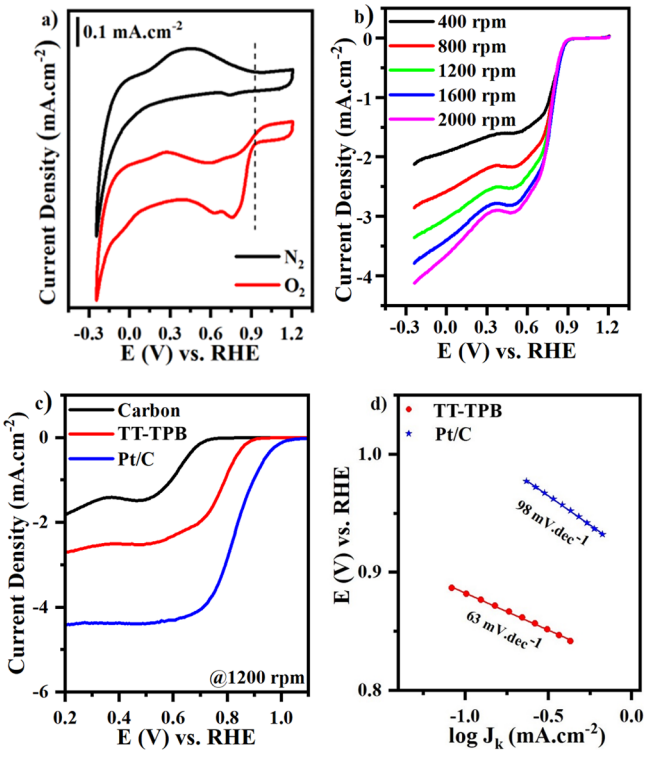

Figure 4. (a) CV curves of the **TT-TPB** electrode in N_2 and O_2 saturated 0.1 M KOH solution at a scan rate of 20 mV/s (b) RDE polarization curves at different rotation rates at a scan rate of 10 mV/s, (c) RDE polarization curves at 1200 rpm of pristine carbon, **TT-TPB**, and Pt/C electrodes, and (d) mass corrected Tafel plots of **TT-TPB** and Pt/C electrodes.

https://doi.org/10.1021/acsaem.2c01830
ACS Appl. Energy Mater. 2022, 5, 13284–13292

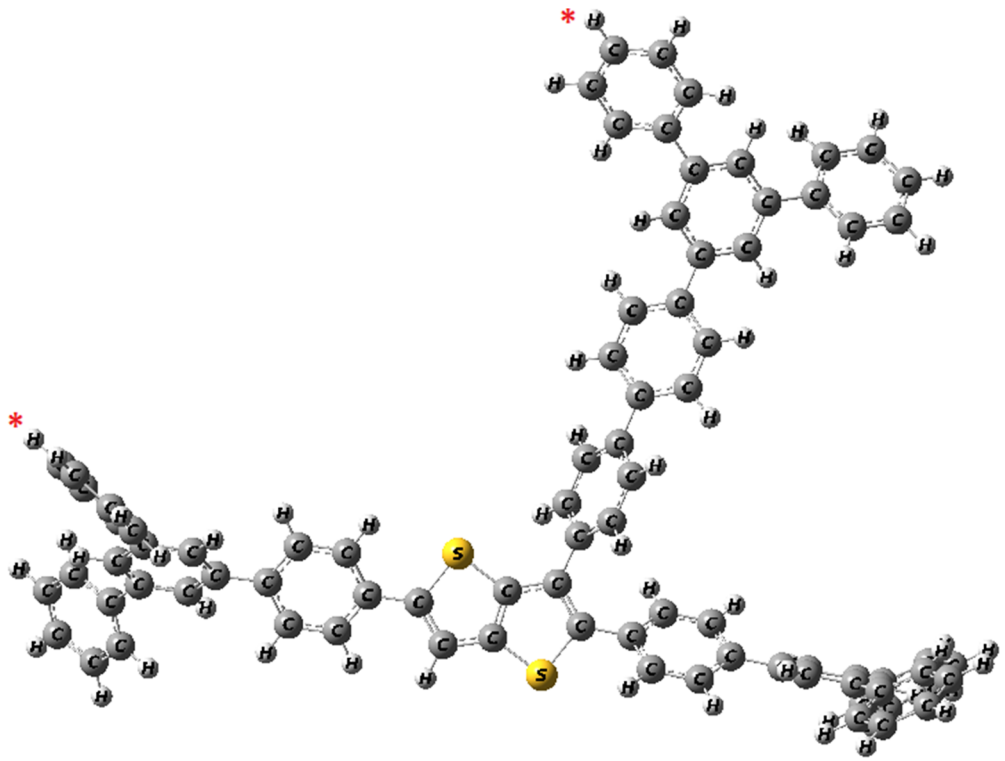

Figure 5. Optimized geometry of **TT-TPB** molecule. The triphenyl groups were found at 19 Å far from each other (with respect to the atoms labeled with an asterisk (*) in the figure).

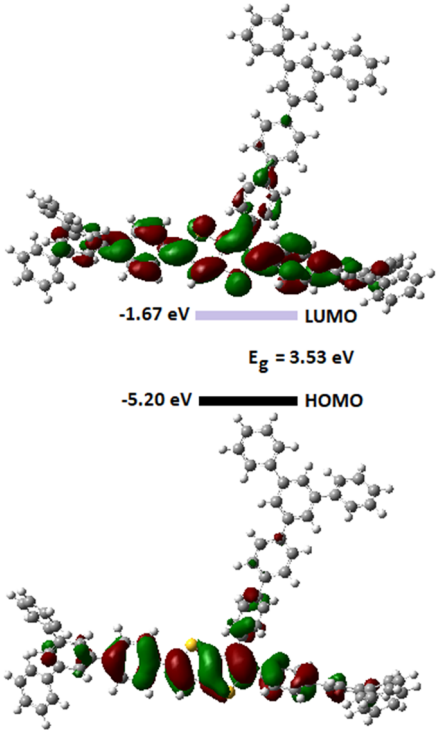

Figure 6. Frontier orbitals and the corresponding energy levels of **TT-TPB**.

Cyclic voltammetry (CV) measurement was performed to investigate the electrochemical properties of **TT-TPB** (Figure 1c). The oxidation and reduction potentials (E_{ox}, E_{red}) were observed to be 1.28 and −1.35 V, respectively. The electrochemical band gap was found to be in good alignment with the optical band gap of **TT-TPB**, which was obtained to be 2.63 eV, using $E_{CV} = E_{ox} - E_{red}$ equation.

Thermal properties of **TT-TPB** were investigated by applying differential scanning calorimetry (DSC) and thermal gravimetric analyses (TGA) under nitrogen flow (Figure 2). DSC analysis of **TT-TPB** showed a high T_g of 136 °C (Figure 2a), and its TGA displayed two gradual endothermic decompositions at 190 °C, which could be due to the release of the trapped solvents in the pores and 600 °C with around 15 and 30% weight losses, respectively. Moreover, with a gradual increase of temperature up to 900 °C, around 65% of **TT-TPB** remained without ash, demonstrating that **TT-TPB** has excellent thermal stability, which is a highly desirable parameter for the preparation of a stable and durable electronic material.

The morphological feature of **TT-TPB** was investigated using scanning electron microscopy (SEM). Considering that the SEM analysis is conducted on a very small area, several images were recorded from different parts at varying magnifications, which indicated a consistent, porous morphology in nanometer size (Figure 3a–d). Through this porous structure, O_2 molecules could easily diffuse and interact with the active sites resulting in noticeable ORR activity.

To evaluate ORR performance of the **TT-TPB** catalyst, CV measurements were conducted in N_2 and O_2 purged KOH (0.1 M) solution, respectively (Figure 4a). A reduction peak at 0.75 V and a broad oxidation peak with a center of 0.45 V vs RHE were obtained in the N_2 purged KOH solution. When oxygen was purged, a new intense peak related to the reduction of oxygen appeared, starting from ≈0.9 V (E_{onset}) and ending at 0.75 V, along with the reduction peak at 0.63 V, where the reduction peak observed at 0.75 V in N_2 shifted to 0.63 V in the presence of oxygen. A similar trend was also observed for the oxidation peak, which shifted from 0.45 to 0.27 V after

https://doi.org/10.1021/acsaem.2c01830
ACS Appl. Energy Mater. 2022, 5, 13284−13292

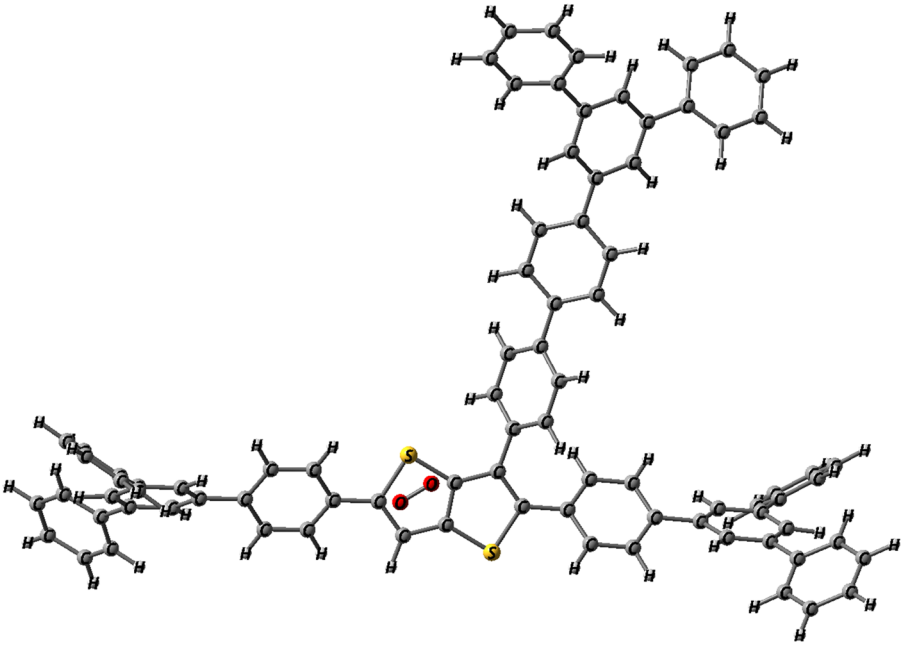

Figure 7. Optimized geometry of the interaction of **TT-TPB** with dioxygen molecule.

purging oxygen. RDE measurements were also conducted at different rotational rates (from 400 to 2000 rpm) to support the activity of **TT-TPB** toward ORR (Figure 4b). As expected, the limiting current density exhibited a typical increase with the rotation rate due to the shortened diffusion layer. The number of transferred electrons during ORR was calculated at different potentials, using the Koutecky−Levich equation deduced from the polarization curves (Figure S4) and applying the RRDE method (Figures S5 and S6). A linear relationship between j^{-1} and $\omega^{-1/2}$ for **TT-TPB** suggested a first-order ORR with respect to dissolved O_2 concentration. Besides, the K-L plots of **TT-TPB** showed parallel straight lines with similar slopes at lower potentials (Figure S4a). However, at high potentials, the K-L plots started to exhibit different slopes through the contribution to the current density from the reduction (broad peak between 0.4 and 0.7 V vs RHE) of carbon powder and **TT-TPB** itself. In alkaline conditions, ORR can occur in a single step over $4e^-$ transfer with a direct reduction of O_2 to OH^-.[60] Alternatively, oxygen can be reduced via an indirect peroxide pathway consisting of two steps. The transferred electrons, calculated for per O_2 molecule from the K-L equation vs potential, are presented in Figure S4b for the **TT-TPB** catalyst. The number of electrons was found to be between 2.6 and 3.2, suggesting a mixture of two- and four-electron mechanisms. Similar electron transfer numbers were obtained applying RRDE method as well, which was supported by the production of HO_2^-% (Figure S6). Although the onset potential of the **TT-TPB** electrode was not as good as commercial Pt/C (≈1 V), it was enhanced from ≈0.73 to ≈0.89−0.9 V ($E_{1/2}$ = 0.8 V) compared to the pristine carbon electrode (Figure 4c). This onset potential was found to be comparable with the literature values (Table S2).[26,61−67] To obtain more information about the ORR mechanism and kinetics, Tafel analysis was employed for the **TT-TPB** and Pt/C electrodes using mass corrected current densities (Figure 4d). The Tafel slope measured with **TT-TPB** was 63 mV/dec, while that obtained with Pt/C was 98 mV/dec. This difference in the Tafel slope values indicated different ORR mechanisms.[68] In addition, the low Tafel slope suggested that the **TT-TPB** catalyst easily adsorbed and activated O_2 on its surface, supporting a strong electrocatalytic performance toward ORR. Stability/durability is one of the key parameters for judging the performance of new ORR electrode catalysts. Figure S7 exhibits a long-term stability measurement of the **TT-TPB** electrode by chronoamperometry at 0.21 V vs RHE in the O_2-saturated KOH solution. After 5 h, a notable decrease in the current density was not observed (decreased from 0.34 mA/cm^2 to 0.3 mA/cm^2).

A further investigation regarding the interaction between O_2 and **TT-TPB** was conducted through theoretical calculations of molecular structure and the related properties on a model **TT-TPB** unit. The global minimum geometry of **TT-TPB** was optimized with density functional theory (DFT) at the B3LYP/6-311G(d,p) level of theory in the Gaussian 16 program package.[69] The optimized structure and the related frontier orbital energy level diagram are given in Figures 5 and 6, respectively.

The triphenylbenzene groups were found to be 19 Å far from each other. The volume of the molecule was calculated to be in an order of 9300 Å^3, and the related properties, i.e., molecular area and the collisional diameter, were predicted as 302 Å^2 and 21.2 Å, respectively (Figure S8). The electron delocalization and electrostatic potential map of the **TT-TPB** system were investigated (Figure S9), along with the calculation of partial atomic charges (Figure S10), the results of which indicated the electrocatalytic activities of the system. The LUMO was found to be delocalized throughout the molecular backbone, demonstrating a good charge-transporting property. Adsorption of O_2 molecule was also modeled and the configuration, in which the dioxygen molecule was adsorbed onto the TT ring of the system, was found to have a minimum energy structure (Figure 7). It may be reasonable to deduce that the electron has to move from the HOMO of **TT-TPB** to the LUMO of the dioxygen molecule. Such an electron transfer looks favorable as the LUMO of O_2 is 0.21 eV lower in energy than that of the HOMO of **TT-TPB**. The condensed f^0

https://doi.org/10.1021/acsaem.2c01830
ACS Appl. Energy Mater. 2022, 5, 13284−13292

Fukui functions, which is accountable for the radical attack, have also been calculated to further investigate the active site of **TT-TPB** (Figure S11). The susceptible moiety for free radical attacks was expected to be the TT unit in the molecular framework. As a consequence, the theoretical results demonstrate that **TT-TPB** material serves as a porous active site for ORR activity and agree with the experimental results.

CONCLUSION

We have demonstrated a design approach for the synthesis of a new conjugated porous polymer (CPP), **TT-TPB**, as a metal-free electrocatalyst, which showed activity toward oxygen reduction reaction (ORR). The structure of the **TT-TPB** polymer, composed of thieno[3,2-*b*]thiophene (TT) donor and triphenylbenzene (TPB) spacer, led to a facile electron transfer throughout the system. Electronic, optical, thermal, and surface properties of the resultant polymer were investigated. The combination of TT and TPB units as a porous structure resulted in remarkable features, i.e., mega Stoke's shift of 112 nm, optical band gap of 2.66 eV, electronic band gap of 2.63 eV, and excellent thermal stability up to 900 °C. Moreover, the porous structure of **TT-TPB** was clarified by scanning electron microscopy (SEM) at different magnitudes ranging from 1 to 20 μm, which was supported by BET measurement. The electrocatalytic activity of **TT-TPB** toward ORR was examined in alkaline media, which exhibited a new intense peak at 0.9 V vs RHE related to oxygen reduction. According to K-L analysis, the ORR took place via mixture of two- and four-electron mechanisms. Besides the experimental and surface measurements, the relevance between O_2 and **TT-TPB**, energy configurations, porous molecular areas, and theoretical calculations were performed on a **TT-TPB** model. The distance between the farthest atoms on the main core and the total volume were calculated as 19 Å and 9300 Å^3, respectively, and the HOMO level of **TT-TPB** was determined to be higher than LUMO level of O_2, proving a perfect porous active side and adsorption of O_2 molecule onto the TT unit. Although the porous material of **TT-TPB** displayed reasonably comparable activity with the materials available in the literature, considering the use of thienothiophene for the first time, the results are considered to be promising. As **TT** is a versatile compound to be modified easily to construct new materials possessing TT, it is hoped that this work could open a new way to construct electrocatalysts with TT and TPB cores as active sites for efficient catalytic reactions in conversion applications.

ASSOCIATED CONTENT

Supporting Information

The Supporting Information is available free of charge at https://pubs.acs.org/doi/10.1021/acsaem.2c01830.

Surface measurement analyses, theoretical calculation analyses, and electrocatalytic analyses (PDF)

AUTHOR INFORMATION

Corresponding Author

Turan Ozturk − *Chemistry Department, Istanbul Technical University, 34469 Istanbul, Turkey; Chemistry Group Laboratories, TUBITAK UME, 41470 Gebze, Kocaeli, Turkey;* orcid.org/0000-0003-3777-5320; Phone: +905358862042; Email: ozturktur@itu.edu.tr

Authors

Recep Isci − *Chemistry Department, Istanbul Technical University, 34469 Istanbul, Turkey;* orcid.org/0000-0003-3086-4478

Timuçin Balkan − *Koç University Tüpraş Energy Center (KUTEM), 34450 Istanbul, Turkey; n2STAR Koç University Nanofabrication and Nanocharacterization Center for Scientific and Technological Advanced Research, 34450 Istanbul, Turkey*

Saeede Tafazoli − *Koç University Tüpraş Energy Center (KUTEM), 34450 Istanbul, Turkey*

Berkay Sütay − *Chemistry Department, Istanbul Technical University, 34469 Istanbul, Turkey*

Mehmet S. Eroglu − *Metallurgical and Materials Engineering Department, Faculty of Engineering, Marmara University, 34854 Istanbul, Turkey; Chemistry Group Laboratories, TUBITAK UME, 41470 Gebze, Kocaeli, Turkey*

Complete contact information is available at: https://pubs.acs.org/10.1021/acsaem.2c01830

Notes

The authors declare no competing financial interest.

ACKNOWLEDGMENTS

We thank Higher Education Council of Turkey (YOK) and TUBITAK grants to R.I. (PhD, 100/2000 YOK and 2211A BIDEP/TUBITAK). The authors thank ITU (Istanbul Technical University) and Unsped Global Lojistik, Turkey, for financial support. We also thank Dr. Sarp Kaya and KUTEM (Koç University Tüpraş Energy Center) for using their infrastructure. T.B. also thanks Kaan Şimşek for his valuable help.

REFERENCES

(1) Hoefler, S. F.; Zettl, R.; Knez, D.; Haberfehlner, G.; Hofer, F.; Rath, T.; Trimmel, G.; Wilkening, H. M. R.; Hanzu, I. New Solar Cell−Battery Hybrid Energy System: Integrating Organic Photovoltaics with Li-Ion and Na-Ion Technologies. *ACS Sustainable Chem. Eng.* **2020**, *8* (51), 19155−19168.

(2) Kabir, E.; Kumar, P.; Kumar, S.; Adelodun, A. A.; Kim, K. H. Solar Energy: Potential and Future Prospects. *Renewable Sustainable Energy Rev.* **2018**, *82*, 894−900.

(3) Xu, L.; Jiang, T.; Lin, P.; Shao, J. J.; He, C.; Zhong, W.; Chen, X. Y.; Wang, Z. L. Coupled Triboelectric Nanogenerator Networks for Efficient Water Wave Energy Harvesting. *ACS Nano* **2018**, *12* (2), 1849−1858.

(4) Lechene, B. P.; Cowell, M.; Pierre, A.; Evans, J. W.; Wright, P. K.; Arias, A. C. Organic solar cells and fully printed super-capacitors optimized for indoor light energy harvesting. *Nano Energy* **2016**, *26*, 631−640.

(5) Liang, J.; Zhu, G.; Lu, Z.; Zhao, P.; Wang, C.; Ma, Y.; Xu, Z.; Wang, Y.; Hu, Y.; Ma, L.; Chen, T.; Tie, Z.; Liu, J.; Jin, Z. Integrated perovskite solar capacitors with high energy conversion efficiency and fast photo-charging rate. *J. Mater. Chem. A* **2018**, *6* (5), 2047−2052.

(6) Panda, C.; Menezes, P. W.; Driess, M. Nano-Sized Inorganic Energy-Materials by the Low-Temperature Molecular Precursor Approach. *Angew. Chem., Int. Ed.* **2018**, *57*, 11130−11139.

(7) Bhanja, P.; Kim, Y.; Paul, B.; Lin, J.; Alshehri, S. M.; Ahamad, T.; Kaneti, Y. V.; Bhaumik, A.; Yamauchi, Y. Facile Synthesis of Nanoporous Transition Metal-Based Phosphates for Oxygen Evolution Reaction. *ChemCatChem* **2020**, *12*, 2091−2096.

(8) Septiani, N. L. W.; Kaneti, Y. V.; Fathoni, K. B.; Kani, K.; Allah, A. E.; Yuliarto, B.; Nugraha; Dipojono, H. K.; Alothman, Z. A.; Golberg, D.; Yamauchi, Y. Self-Assembly of Two-Dimensional Bimetallic Nickel−Cobalt Phosphate Nanoplates into One-Dimen-

sional Porous Chainlike Architecture for Efficient Oxygen Evolution Reaction. *Chem. Mater.* **2020**, *32*, 7005−7018.
(9) Pu, Z.; Zhao, J.; Amiinu, I. S.; Li, W.; Wang, M.; He, D.; Mu, S. A Universal Synthesis Strategy for P-Rich Noble Metal Diphosphide Based Electrocatalysts for the Hydrogen Evolution Reaction. *Energy Environ. Sci.* **2019**, *12*, 952−957.
(10) Liu, Q.; Su, X.; Lei, D.; Qin, Y.; Wen, J.; Guo, F.; Wu, Y. A.; Rong, Y.; Kou, R.; Xiao, X.; Aguesse, F.; Bareño, J.; Ren, Y.; Lu, W.; Li, Y. Approaching the capacity limit of lithium cobalt oxide in lithium ion batteries via lanthanum and aluminium doping. *Nat. Energy.* **2018**, *3* (11), 936−943.
(11) Liu, Z.; Wang, J.; Lu, B. Plum pudding model inspired KVPO4F@3DC as high-voltage and hyperstable cathode for potassium ion batteries. *Science Bulletin* **2020**, *65* (15), 1242−1251.
(12) Kulkarni, A.; Siahrostami, S.; Patel, A.; Nørskov, J. K. Understanding catalytic activity trends in the oxygen reduction reaction. *Chem. Rev.* **2018**, *118* (5), 2302−2312.
(13) Zhang, C.; Hwang, S. Y.; Trout, A.; Peng, Z. Solid-state chemistry-enabled scalable production of octahedral Pt−Ni alloy electrocatalyst for oxygen reduction reaction. *J. Am. Chem. Soc.* **2014**, *136* (22), 7805−7808.
(14) Mukherjee, D.; P, M. A.; Sampath, S. Few-Layer Iron Selenophosphate, $FePSe_3$: Efficient Electrocatalyst Towards Water Splitting and Oxygen Reduction Reactions. *ACS Appl. Energy Mater.* **2018**, *1*, 220−231.
(15) Mecheri, B.; Gokhale, R.; Santoro, C.; Costa de Oliveira, M. A.; D'Epifanio, A.; Licoccia, S.; Serov, A.; Artyushkova, K.; Atanassov, P. Oxygen Reduction Reaction Electrocatalysts Derived from Iron Salt and Benzimidazole and Aminobenzimidazole Precursors and Their Application in Microbial Fuel Cell Cathodes. *ACS Appl. Energy Mater.* **2018**, *1* (10), 5755−5765.
(16) Abbas, M. A.; Bang, J. H. Rising Again: Opportunities and Challenges for Platinum-Free Electrocatalysts. *Chem. Mater.* **2015**, *27* (21), 7218−7235.
(17) Sealy, C. The problem with platinum. *Mater. Today* **2008**, *11* (12), 65−68.
(18) Kim, J.; Hong, Y.; Lee, K.; Kim, J. Y. High. *Adv. Energy Mater.* **2020**, *10*, 2002049.
(19) Inamdar, A. I.; Chavan, H. S.; Hou, B.; Lee, C. H.; Lee, S. U.; Cha, S.; Kim, H.; Im, H. A Robust Nonprecious CuFe Composite as a Highly Efficient Bifunctional Catalyst for Overall Electrochemical Water Splitting. *Small* **2020**, *16*, 1905884.
(20) Zhang, S. L.; Guan, B. Y.; Lou, X. W. D. Co-Fe Alloy/N-Doped Carbon Hollow Spheres Derived from Dual Metal−Organic Frameworks for Enhanced Electrocatalytic Oxygen Reduction. *Small* **2019**, *15*, 1805324.
(21) Wang, H.; Chen, B.-H.; Liu, D.-J. Metal-Organic Frameworks and Metal-Organic Gels for Oxygen Electrocatalysis: Structural and Compositional Considerations. *Adv. Mater.* **2021**, *33*, 2008023.
(22) Long, X.; Li, D.; Wang, B.; Jiang, Z.; Xu, W.; Wang, B.; Yang, D.; Xia, Y. Heterocyclization Strategy for Construction of Linear Conjugated Polymers: Efficient Metal-Free Electrocatalysts for Oxygen Reduction. *Angew. Chem., Int. Ed. Engl.* **2019**, *58*, 11369−11373.
(23) Ma, L.; Liu, Y.; Liu, Y.; Jiang, S.; Li, P.; Hao, Y.; Shao, P.; Yin, A.; Feng, X.; Wang, B. Ferrocene-Linkage-Facilitated Charge Separation in Conjugated Microporous Polymers. *Angew. Chem., Int. Ed. Engl.* **2019**, *58*, 4221−4226.
(24) Geng, K.; He, T.; Liu, R.; Dalapati, S.; Tan, K. T.; Li, Z.; Tao, S.; Gong, Y.; Jiang, Q.; Jiang, D. Covalent Organic Frameworks: Design, Synthesis, and Functions. *Chem. Rev.* **2020**, *120*, 8814−8933.
(25) Kandambeth, S.; Dey, K.; Banerjee, R. Covalent organic frameworks: chemistry beyond the structure. *J. Am. Chem. Soc.* **2019**, *141*, 1807−1822.
(26) Bhattacharyya, S.; Samanta, D.; Roy, S.; Haveri Radhakantha, V. P.; Maji, T. K. In situ Stabilization of Au and Co Nanoparticles in a Redox-Active Conjugated Microporous Polymer Matrix: Facile Heterogeneous Catalysis and Electrocatalytic Oxygen Reduction Reaction Activity. *ACS Appl. Mater. Interfaces* **2019**, *11* (5), 5455−5461.
(27) Yan, S.; Guan, X.; Li, H.; Li, D.; Xue, M.; Yan, Y.; Valtchev, V.; Qiu, S.; Fang, Q. Three-Dimensional Salphen-Based Covalent-Organic Frameworks as Catalytic Antioxidants. *J. Am. Chem. Soc.* **2019**, *141*, 2920−2924.
(28) Ding, S. Y.; Wang, W. Covalent Organic Frameworks (COFs): From Design to Applications. *Chem. Soc. Rev.* **2013**, *42*, 548−568.
(29) Zhang, P.; Weng, Z.; Guo, J.; Wang, C. Solution-Dispersible, Colloidal, Conjugated Porous Polymer Networks with Entrapped Palladium Nanocrystals for Heterogeneous Catalysis of the Suzuki-Miyaura Coupling Reaction. *Chem. Mater.* **2011**, *23*, 5243−5249.
(30) Isci, R.; Tekin, E.; Kaya, K.; Mucur, S. P.; Gorkem, S. F.; Ozturk, T. Tetraphenylethylene substituted thienothiophene and dithienothiophene derivatives: synthesis, optical properties and OLED applications. *J. Mater. Chem. C* **2020**, *8*, 7908−7915.
(31) Isci, R.; Tekin, E.; Mucur, S. P.; Ozturk, T. A Bifunctional Bulky Thienothiophene Derivative; Synthesis, Electronic-Optical Properties and OLED Applications. *ChemistrySelect* **2020**, *5*, 13091−13098.
(32) Isci, R.; Gunturkun, D.; Yalin, A. S.; Ozturk, T. Copolymers of 4-thieno[3,2-*b*]thiophen-3-ylbenzonitrile with anthracene and biphenyl; synthesis, characterization, electronic, optical, and thermal properties. *J. Polym. Sci.* **2021**, *59*, 117−123.
(33) Isci, R.; Unal, M.; Kucukcakir, G.; Gurbuz, N. A.; Gorkem, S. F.; Ozturk, T. Triphenylamine/4,4′-Dimethoxytriphenylamine-Functionalized Thieno[3,2-*b*]thiophene Fluorophores with a High Quantum Efficiency: Synthesis and Photophysical Properties. *J. Phys. Chem. B* **2021**, *125*, 13309−13319.
(34) Isci, R.; Varzeghani, A. R.; Kaya, K.; Sütay, B.; Tekin, E.; Ozturk, T. Triphenylamine/Tetraphenylethylene Substituted 4-Thieno[3,2-*b*]thiophen-3-ylbenzonitriles: Synthesis, Photophysical-Electronic Properties, and Applications. *ACS Sustainable Chem. Eng.* **2022**, *10* (4), 1605−1615.
(35) Gunturkun, D.; Isci, R.; Sütay, B.; Majewski, L. A.; Faraji, S.; Ozturk, T. Copolymers of 3-Arylthieno[3,2-*b*]thiophenes Bearing Different Substituents: Synthesis, Electronic, Optical, Sensor and Memory Properties. *Eur. Polym. J.* **2022**, *170*, 111167.
(36) Topal, S.; Isci, R.; Sezer, E.; Ozturk, T.; Ustamehmetoglu, B. Synthesis and electropolymerization of 3-arylthieno[3,2-*b*]thiophenes and triphenylamine based comonomers. *Electrochim. Acta* **2021**, *389*, 138688.
(37) Mishra, A.; Ma, C.-Q.; Bäuerle, P. Functional Oligothiophenes: Molecular Design for Multidimensional Nanoarchitectures and Their Applications. *Chem. Rev.* **2009**, *109*, 1141−1276.
(38) Tang, W.; Ke, L.; Tan, L.; Lin, T.; Kietzke, T.; Chen, Z.-K. Conjugated Copolymers Based on Fluorene−Thieno[3,2-b]-thiophene for Light-Emitting Diodes and Photovoltaic Cells. *Macromolecules* **2007**, *40*, 6164−6171.
(39) Turksoy, F.; Wallis, J. D.; Tunca, U.; Ozturk, T. An in depth study of the formation of new tetrathiafulvalene derivatives from 1,8-diketones. *Tetrahedron* **2003**, *59* (41), 8107−8116.
(40) Bildirir, H.; Osken, I.; Ozturk, T.; Thomas, A. Reversible Doping of a Dithienothiophene-Based Conjugated Microporous Polymer. *Chem.—Eur. J.* **2015**, *21* (26), 9306−9311.
(41) Bildirir, H.; Osken, I.; Schmidt, J.; Ozturk, T.; Thomas, A. Chemical RedOx Properties of a Donor-Acceptor Conjugated Microporous Dithienothiophene-Benzene co-Polymer Formed via Suzuki-Miyaura Cross-coupling. *ChemistrySelect* **2016**, *1* (4), 748−751.
(42) Osken, I.; Sahin, O.; Gundogan, A. S.; Bildirir, H.; Capan, A.; Ertas, E.; Eroglu, M. S.; Wallis, J. D.; Topal, K.; Ozturk, T. Selective syntheses of vinylenedithiathiophenes (VDTTs) and dithieno[2,3-b;2′,3′-d]thiophenes (DTTs); building blocks for π-conjugated systems. *Tetrahedron* **2012**, *68* (4), 1216−1222.
(43) Tavasli, A.; Gurunlu, B.; Gunturkun, D.; Isci, R.; Faraji, S. A Review on Solution-Processed Organic Phototransistors and Their Recent Developments. *Electronics* **2022**, *11* (3), 316.

(44) Bronstein, H.; Chen, Z.; Ashraf, R. S.; Zhang, W.; Du, J.; Durrant, J. R.; Shakya Tuladhar, P.; Song, K.; Watkins, S. E.; Geerts, Y.; Wienk, M. M.; Janssen, R. A. J.; Anthopoulos, T.; Sirringhaus, H.; Heeney, M.; McCulloch, I. Thieno[3,2-*b*]thiophene-Diketopyrrolopyrrole-Containing Polymers for High-Performance Organic Field-Effect Transistors and Organic Photovoltaic Devices. *J. Am. Chem. Soc.* **2011**, *133*, 3272−3275.
(45) Vishnoi, P.; Kaleeswaran, D.; Murugavel, R. 1,3,5-Triphenylbenzene: a versatile photoluminescent chemo-sensor platform and supramolecular building block. *RSC Adv.* **2018**, *8*, 17535−17550.
(46) Mejuto, C.; Guisado-Barrios, G.; Peris, E. Novel Rhodium and Iridium Complexes Coordinated to C3-Symmetric Tris-NHC Ligands Based on a 1,3,5-Triphenylbenzene Core. Electronic and Catalytic Properties. *Organometallics* **2014**, *33* (12), 3205−3211.
(47) Wang, L.; Wan, Y.; Ding, Y.; Wu, S.; Zhang, Y.; Zhang, X.; Zhang, G.; Xiong, Y.; Wu, X.; Yang, J.; Xu, H. Conjugated Microporous Polymer Nanosheets for Overall Water Splitting Using Visible Light. *Adv. Mater.* **2017**, *29*, 1702428.
(48) Edhborg, F.; Bildirir, H.; Bharmoria, P.; Moth-Poulsen, K.; Albinsson, B. Intramolecular Triplet-Triplet Annihilation Photon Upconversion in Diffusionally Restricted Anthracene Polymer. *J. Phys. Chem. B* **2021**, *125*, 6255−6263.
(49) Zhang, L.; Sun, J.-S.; Sun, F.; Chen, P.; Liu, J.; Zhu, G. Facile Synthesis of Ultrastable Porous Aromatic Frameworks by Suzuki−Miyaura Coupling Reaction for Adsorption Removal of Organic Dyes. *Chem. -Eur. J.* **2019**, *25*, 3903−3908.
(50) Dai, C.; Zhong, L.; Wu, W.; Zeng, C.; Deng, Y.; Li, S. 1,3,5-Triphenylbenzene Based Porous Conjugated Polymers for Highly Efficient Photoreduction of Low-Concentration CO2 in the Gas-Phase System. *Sol. RRL* **2022**, *6*, 2100872.
(51) Zhang, X.; Zhang, Q.; Cui, J.; Yan, J.; Liu, J.; Wu, Y. New insights into the key bifunctional role of sulfur in Fe−N−C single-atom catalysts for ORR/OER. *Nanoscale* **2022**, *14*, 3212−3223.
(52) Kiciński, W.; Dembinska, B.; Norek, M.; Budner, B.; Polański, M.; Kulesza, P. J.; Dyjak, S. Heterogeneous iron-containing carbon gels as catalysts for oxygen electroreduction: Multifunctional role of sulfur in the formation of efficient systems. *Carbon* **2017**, *116*, 655−669.
(53) Wang, H.; Bo, X.; Zhang, Y.; Guo, L. Sulfur-doped ordered mesoporous carbon with high electrocatalytic activity for oxygen reduction. *Electrochim. Acta* **2013**, *108*, 404−411.
(54) Li, F.; Sun, L.; Luo, Y.; Li, M.; Xu, Y.; Hu, G.; Li, X.; Wang, L. Effect of thiophene S on the enhanced ORR electrocatalytic performance of sulfur-doped graphene quantum dot/reduced graphene oxide nanocomposites. *RSC Adv.* **2018**, *8* (35), 19635−19641.
(55) Goncalves, J. P.; de Oliveira, C. C.; da Silva Trindade, E.; Riegel-Vidotti, I. C.; Vidotti, M.; Simas, F. F. In vitro biocompatibility screening of a colloidal gum Arabic-polyaniline conducting nanocomposite. *Int. J. Biol. Macromol.* **2021**, *173*, 109−117.
(56) Jonas, F.; Guntermann, U. U.S. Patent 6,358,437. U.S. Patent and Trademark Office: Washington, DC, 2002.
(57) Jin, Z.; Nie, H.; Yang, Z.; Zhang, J.; Liu, Z.; Xu, X.; Huang, S. Metal-free selenium doped carbon nanotube/graphene networks as a synergistically improved cathode catalyst for oxygen reduction reaction. *Nanoscale* **2012**, *4*, 6455−6460.
(58) Zhou, R.; Zheng, Y.; Jaroniec, M.; Qiao, S. Z. Determination of the Electron Transfer Number for the Oxygen Reduction Reaction: From Theory to Experiment. *ACS Catal.* **2016**, *6* (7), 4720−4728.
(59) Sarapuu, A.; Hussain, S.; Kasikov, A.; Pollet, B. G.; Tammeveski, K. Electroreduction of oxygen on Nafion®-coated thin platinum films in acid media. *J. Electroanal. Chem.* **2019**, *848*, 113292.
(60) Kim, H. W.; Bukas, V. J.; Park, H.; Park, S.; Diederichsen, K. M.; Lim, J.; Cho, Y. H.; Kim, J.; Kim, W.; Han, T. H.; Voss, J.; Luntz, A. C.; McCloskey, B. D. Mechanisms of Two-Electron and Four-Electron Electrochemical Oxygen Reduction Reactions at Nitrogen-Doped Reduced Graphene Oxide. *ACS Catal.* **2020**, *10*, 852−863.
(61) McDonnell, L. P; Viner, J. J. S.; Ruiz-Tijerina, D. A; Rivera, P.; Xu, X.; Fal'ko, V. I; Smith, D. C Superposition of intra- and inter-layer excitons in twistronic $MoSe_2/WSe_2$ bilayers probed by resonant Raman scattering. *2D Mater.* **2021**, *8*, 035009.
(62) Lu, G.; Yang, H.; Zhu, Y.; Huggins, T.; Ren, Z. J.; Liu, Z.; Zhang, W. Synthesis of a conjugated porous Co(ii) porphyrinylene−ethynylene framework through alkyne metathesis and its catalytic activity study. *J. Mater. Chem. A* **2015**, *3*, 4954−4959.
(63) Ren, S.-B.; Chen, X.-L.; Li, P.-X.; Hu, D.-Y.; Liu, H.-L.; Chen, W.; Xie, W.-B.; Chen, Y.; Yang, X.-L.; Han, D.-M.; Ning, G.-H.; Xia, X.-H. Nitrogen and sulfur dual-doped carbon nanotube derived from a thiazolothiazole based conjugated microporous polymer as efficient metal-free electrocatalysts for oxygen reduction reaction. *J. Power Sources* **2020**, *461*, 228145.
(64) Roy, S.; Bandyopadhyay, A.; Das, M.; Ray, P. P.; Pati, S. K.; Maji, T. K. Redox-active and semi-conducting donor-acceptor conjugated microporous polymers as metal-free ORR catalysts. *J. Mater. Chem. A* **2018**, *6*, 5587−5591.
(65) Li, Y.; Tao, X.; Wei, J.; Lv, X.; Wang, H. Metal phthalocyanine-porphyrin-based conjugated microporous polymer derived bifunctional electrocatalysts for Zn-air batteries. *Asian J. Chem.* **2020**, *15*, 1970−1975.
(66) Jayanthi, S.; Muthu, D. V. S.; Jayaraman, N.; Sampath, S.; Sood, A. K. Semiconducting Conjugated Microporous Polymer: An Electrode Material for Photoelectrochemical Water Splitting and Oxygen Reduction. *ChemistrySelect* **2017**, *2* (16), 4522−4532.
(67) Liu, W.; Wang, K.; Wang, C.; Liu, W.; Pan, H.; Xiang, Y.; Qi, D.; Jiang, J. Mixed Phthalocyanine-Porphyrin-Based Conjugated Microporous Polymers towards Unveiling the Activity Origin of Fe-N4 Catalysts for Oxygen Reduction Reaction. *J. Mater. Chem. A* **2018**, *6*, 22851−22857.
(68) Fernandes, D. M.; Novais, H. C.; Bacsa, R.; Serp, P.; Bachiller-Baeza, B.; Rodríguez-Ramos, I.; Guerrero-Ruiz, A.; Freire, C. Polyoxotungstate@Carbon Nanocomposites As Oxygen Reduction Reaction (ORR) Electrocatalysts. *Langmuir* **2018**, *34*, 6376−6387.
(69) Frisch, M. J.; Trucks, G. W.; Schlegel, H. B.; Scuseria, G. E.; Robb, M. A.; Cheeseman, J. R.; Scalmani, G.; Barone, V.; Petersson, G. A.; Nakatsuji, H.; Li, X.; Caricato, M.; Marenich, A. V.; Bloino, J.; Janesko, B. G.; Gomperts, R.; Mennucci, B.; Hratchian, H. P.; Ortiz, J. V.; Izmaylov, A. F.; Sonnenberg, J. L.; Williams-Young, D.; Ding, F.; Lipparini, F.; Egidi, F.; Goings, J.; Peng, B.; Petrone, A.; Henderson, T.; Ranasinghe, D.; Zakrzewski, V. G.; Gao, J.; Rega, N.; Zheng, G.; Liang, W.; Hada, M.; Ehara, M.; Toyota, K.; Fukuda, R.; Hasegawa, J.; Ishida, M.; Nakajima, T.; Honda, Y.; Kitao, O.; Nakai, H.; Vreven, T.; Throssell, K.; Montgomery, J. A., Jr.; Peralta, J. E.; Ogliaro, F.; Bearpark, M. J.; Heyd, J. J.; Brothers, E. N.; Kudin, K. N.; Staroverov, V. N.; Keith, T. A.; Kobayashi, R.; Normand, J.; Raghavachari, K.; Rendell, A. P.; Burant, J. C.; Iyengar, S. S.; Tomasi, J.; Cossi, M.; Millam, J. M.; Klene, M.; Adamo, C.; Cammi, R.; Ochterski, J. W.; Martin, R. L.; Morokuma, K.; Farkas, O.; Foresman, J. B.; Fox, D. J.*Gaussian 16*, revision C.01; Gaussian, Inc.: Wallingford, CT, 2016.

https://doi.org/10.1021/acsaem.2c01830
ACS Appl. Energy Mater. 2022, 5, 13284−13292